Hindawi
International Journal of RF and Microwave Computer-Aided Engineering
Volume 2024, Article ID 9040638, 10 pages
https://doi.org/10.1155/2024/9040638

Research Article

Simple Integration of Cavity-Backed Antenna with Patch Antenna for Developing Hybrid Antenna Using SIW Technology

A. H. Murshed[1], **M. A. Hossain**[1], **N. K. Kiem**[2], **N. H. Hai**[2], **E. Nishiyama**[3], **I. Toyoda**[3] **and I. Mahbub**[4]

[1]*Department of Electronics and Telecommunication Engineering, Chittagong University of Engineering and Technology, Chattogram 4349, Bangladesh*
[2]*Faculty of Communication Engineering, School of Electrical and Electronics Engineering, Hanoi University of Science and Technology, Hanoi 10000, Vietnam*
[3]*Department of Electrical and Electronic Engineering, Saga University, Saga 840-8502, Japan*
[4]*Department of Electrical and Computer Engineering, The University of Texas at Dallas, Richardson, USA*

Correspondence should be addressed to M. A. Hossain; azad@cuet.ac.bd

Received 11 June 2023; Revised 14 October 2023; Accepted 14 December 2023; Published 6 February 2024

Academic Editor: Ravi Gangwar

This paper proposes a novel scheme for developing a linearly polarized (LP) hybrid antenna using a simple integration of a planner cavity-backed antenna with a conventional rectangular patch antenna. To substantiate, a half-mode rectangular substrate-integrated waveguide technique is divided into halves to reduce the size and later integrated with a patch antenna. The patch antenna is getting excited by the mutual coupling of TE_{101} mode and resonating in the vicinity of the cavity resonator. These two different combinations of strategy let the antenna obtain superior characteristics such as bandwidth and gain. To make this structure enable to use in the planner circuit, a 50 Ω microstrip line is incorporated. This proposed hybrid antenna is simulated and tested experimentally to justify its worthiness. The simulated and measured data maintained good agreements regarding S_{11}, bandwidth, gain, radiation pattern, and efficiency.

1. Introduction

As of late, microstrip antenna has been very popular for its low profile, lightweight, low cost, and easy integration with the planner circuit, which draws the researcher's attention and causes drastic improvement in the antenna field. However, suffering from low bandwidth (BW), low gain, and efficiency has been the prime concern, and many techniques have emerged to grapple with the mentioned problems. As a result, many BW enhancement techniques, such as partial ground plane technique [1–6], thick substrate [7, 8], aperture coupled [9, 10], and multilayer techniques [11, 12], are used. Among them is the partial ground plane technique, which provides a low-gain bidirectional radiation pattern with wide BW behaviour. Thick substrate waxes the antenna's thickness; aperture-coupled increase fabrication complexity and multilayer techniques are often byzantine in terms of fabrication complexity.

On the other hand, an array antenna could reduce backward radiation while expanding broadside radiation. Conversely, 0.8λ spacing between elements in the both-sided MIC technique demands larger space and, in the conventional technique, introduces a loss in the transmission line [13–16]. Furthermore, the conductor loss is prime in a microstrip antenna; a bidirectional radiation pattern wreaked backward radiation in a slot antenna. To decipher this, a metal reflector or cavity-backed antenna is a way out of curbing backward radiation. That said, in a metal reflector antenna, $\lambda/4$ spacing is needed between the antenna and sheet; the same spacing is also used as depth in conventional array antenna to make this antenna operate. Consequently, the above-mentioned techniques make them

bulky, heavy, and expensive, making them not eligible for employment in the planner circuit proposed in [17–20].

In an attempt to figure this problem out, substrate-integrated waveguide (SIW) has been a prominent candidate. A typical SIW resonator [21–24] allows the miniaturization of a cavity-backed antenna by allowing it to be integrated with a planner circuit with a microstrip line or a planner structure like a typical patch antenna. Thus, it is possible to get advantages of both structures. That was made possible by the SIW technique, which can mimic the properties of a typical resonator or waveguide to realize printed circuit board technology by employing rows of vias or holes in a dielectric substrate. Recently, they have been treated as a low-cost microwave component in microwave circuit suitable for operating at high frequency and show multiband characteristics and high front-to-back ratio (FTBR) [25–28]. Although being able to be integrated into a planner antenna, the SIW antenna suffers from the large size. Hence, miniaturization of SIW is needed with elevated efficiency and operation. Antenna fractal geometry can be suitable for miniaturization, BW, and gain enhancement [29]. Such antenna shows promising results despite minimized size; however, mechanical limitations make them unsuitable for fabrication. Besides, to enhance gain, multiple arrays of SIW elements are proposed where isolation between elements becomes the prime concern along with multiple SMA connector ports, complicating antenna manufacturing and overall size [30]. Consequently, miniaturization is proposed by dividing SIW along its magnetic wall [31–35].

The half-mode substrate-integrated waveguide (HMSIW) technique is proposed in [32] and the quarter-mode substrate-integrated waveguide (QMSIW) in [33, 34]. Similarly, eighth-mode SIW (EMSIW) is proposed for wearable applications [35]. However, their natural configuration because of possessing metallic rows allows them to attain a narrow BW, i.e., high Q-factor, less lossy, and high-power handler; some are reported in [36]. For example, a self-diplexing [37] and self-triplexing [38] antenna based on SIW is proposed. Such an [32–35, 37, 38] antenna is divested of wide BW behaviour for high Q-value. A SIW antenna with a partial ground plane is proposed to curtail the Q-factor [39]. However, such a scheme may not be compatible with many antenna applications, a Fabry-Perot cavity system [40], for not having a full-plane ground. Additionally, a multilayer of SIW is proposed [41] for BW enhancement of SIW-based antenna, in which a multilayer scheme may not be compatible with many microwave circuits.

However, placing an extra resonator outside by merging the operating frequency would address the above-mentioned problem. This can be done without even increasing the antenna's overall size. An instance of this is an antenna in [42, 43], known as a hybrid antenna, where an array of parasitic patches is used in [42] to escalate the BW of the rectangular HMSIW cavity. Note that patches of the array further cause an improvement in gain and other parameters. The experimental validation of the patch array is provided in [42]; however, no experimental data is provided for a single patch with HMSIW. This paper is aimed at providing an in-depth analysis with proper experimental validation of that hybrid antenna, single patch with HMSIW cavity. Furthermore, in contrast to the TE_{100} mode analysis of a hybrid antenna (joint combination of a single patch with a circular HMSIW cavity) [43], this paper investigates the TE_{101} mode of a hybrid antenna since the proposed rectangular cavity solely excites the TE_{101} mode.

Such structure [42, 43] can provide wide BW behaviour, and depending upon the requirement, careful design, and substrate specification, UWB behaviour can be obtained. A typical wideband antenna utilizes the operating spectrum efficiently in radar systems with a high spatial resolution for defense systems [44], mobile phones, and many handy devices [45, 46]. In addition, it can be used in numerous types of biomedical applications, including heartbeat monitoring [47]. Recently, SIW-backed antenna has been employed for full-duplex communication system and to develop efficient hybrid-filter subsystem [48, 49].

In this paper, a planner cavity-backed hybrid antenna is proposed, theoretically analyzed, and tested experimentally, which is compounded from HMSIW cavity and patch antenna to reduce the Q-factor. This technique is nothing but a simple manifestation of a multiresonator on a single substrate to enhance BW. Firstly, the HMSIW technique reduces the size, which supports the dominant mode TE_{101} within the cavity. Secondly, adding an extra patch coupled with electromagnetic induction proved effective for improving other antenna parameters. Eventually, the proposed antenna ended up being a hybrid high FTBR wideband antenna, which BW and gain marked the improvement in the comparison table (Table 1) compared to previously published cavity-backed antennas.

2. Antenna Configurations

2.1. Developing HMSIW Antenna. Initially, a full-mode substrate-integrated waveguide (FMSIW) is constructed in Figure 1(a) and then simulated to carefully observe its magnetic field distribution in Figure 1(b). Later, by dividing into halves alongside the A-B axis, known as the perfect magnetic wall (PMW), two semirectangular cavity antennas rendering almost the same electric field distribution can be formed. This semirectangular cavity is a half-mode cavity, also known as HMSIW. Figure 2 shows an HMSIW antenna, $17 \times 18\,mm^2$ in size, where the open edge (perfect magnetic wall) acts as radiating aperture. An inset microstrip feed has been proposed, and the radiation mechanism in terms of an electric and magnetic field of the HMSIW antenna is shown in Figure 2. The HMSIW antenna has a dielectric aperture through which it radiates in free space. The simulated reflection coefficient, S_{11}, is shown in Figure 3(a), along with its gain and radiation efficiency. The dielectric aperture is 4.40 mm in length. The operating frequency has not changed so much in HMSIW as it renders an electric field almost half that of FMSIW. The S_{11} is better than -25 dB, which implies that the antenna is able to receive the RF energy from a feed. Its corresponding input impedance curve on the Smith chart passes over the prime center of the unity axis, which suggests good impedance matching. It possesses a -10 dB BW of only 160 MHz with a neat gain of 6.83 dBi in Figure 3(a), which is

Table 1: A comparison with previously published papers.

Prop.	Thickness	Gain (dBi)	BW (%)	FTBR (dB)	ε_r	Band and feed
[25]	0.02 λ_g	5.5/5.5	1.8/2.1	20.8/18.1	2.22	ML
[26]	0.03 λ_g	5.3/4.3	2.02/1.52	14/16	2.22	X, Ku; ML
[27]	0.07 λ_g	4.9/6.1	1.4/5.9	18/18	2.2	SIW, ML
[28]	0.02 λ_g	5.4	1.7	16.1	2.2	X; ML
[38]	0.02 λ_g	4.5/4.9/6.1	2.0/1.9/1.7	14	2.2	C; 3-ML
[37]	0.05 λ_g	5.6/5.9	1.9/3.7	16.9	2.2	X, Ku; ML
[32]	0.03 λ_g	5.15/5.5	NM	>10	2.22	C; ML
[33]	0.03 λ_g	4.8/5.7	NM	20	2.22	S; ML
[34]	0.13 λ_g	4.9/5.3	1.9/5.3	25.6/24	3.55	S, C; ML
[prop.]	0.05 λ_g	6.45	3.46	23.3	3.55	Ku; ML

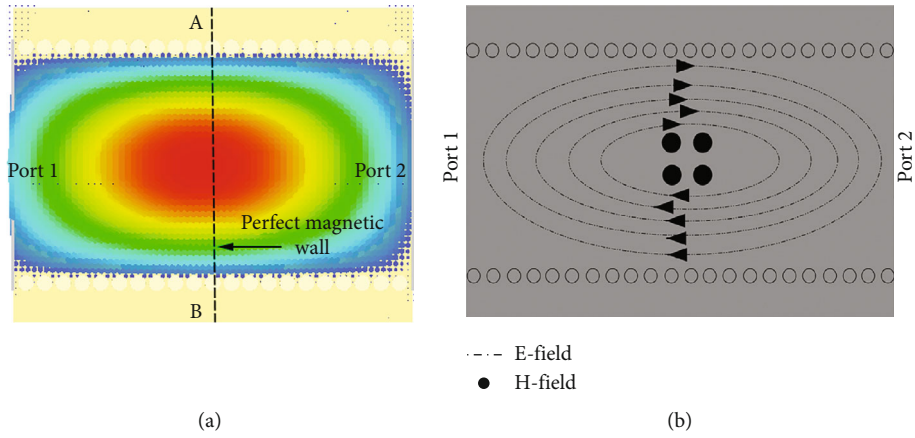

Figure 1: (a) The simulated electric field distribution of the rectangular SIW resonator at the fundamental frequency and (b) TE_{101} electric field distribution across the rectangular SIW.

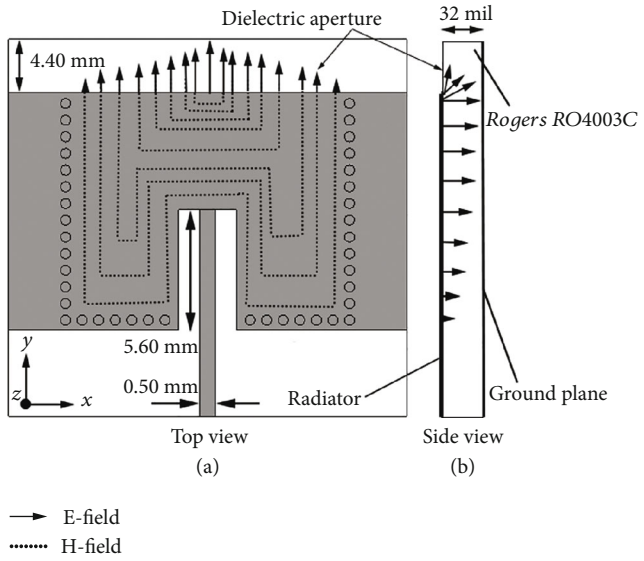

Figure 2: The HMSIW antenna with TE_{101} electric field distribution across the cavity: (a) top view and (b) side view.

insufficient and less than reported in [25–28, 32, 37, 38]. The simulated radiation efficiency was 70% for the HMSIW antenna.

In addition, the simulated normalized radiation pattern is shown in terms of both E-plane (E_θ in $\varphi = 90°$) and H-plane (E_θ in $\varphi = 0°$) of the proposed HMSIW cavity-backed antenna in Figure 3(b), which is quite directional. The E-plane (E_θ in $\varphi = 90°$) radiation pattern is symmetric as antennas YZ-axis. The E-plane pattern points at 0° bore-sight direction with an SLL of -8.4 dB. Conversely, the H-plane (E_θ in $\varphi = 0°$) leading beam points at a 27° broadside direction with minimized sidelobe level (SLL) of -7.2 dB. Besides, the antenna shows a good cross-polarization (XPL) level of less than -12 dBi on the E-plane and less than -14 dBi on the H-plane.

2.2. Hybrid Antenna as a Combination of HMSIW Antenna and Patch Antenna and Its Operation. The rectangular patch antenna in Figure 4, which acts as a coresonator, is placed near the radiating edge of the HMSIW antenna in Figure 5(a). The antenna's aperture increases, resulting in an increment in radiation while decreasing the antenna's

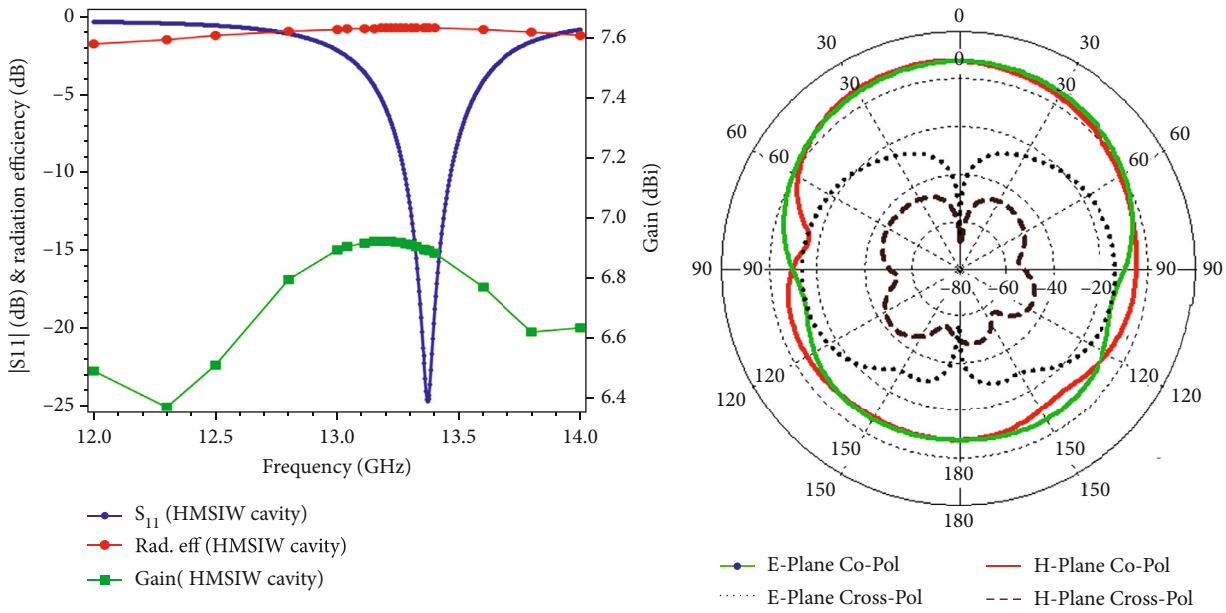

FIGURE 3: (a) The simulated S_{11}, radiation efficiency, and gain of the HMSIW antenna and (b) the normalized simulated radiation patterns of HMSIW antenna in terms of E-plane (YZ cut) and H-plane (XZ cut) at 13.37 GHz.

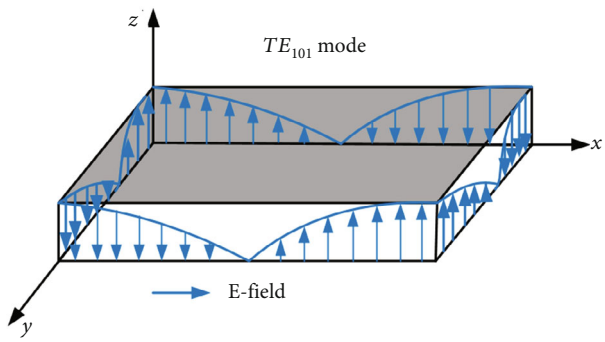

FIGURE 4: The TE_{101} field distribution inside the patch antenna.

overall impedance. This causes a left shift of antenna input impedance in the Smith chart. Therefore, the antenna's inset feed length is shortened than that of HMSIW in Figure 2 to make the input impedance pass over the prime center, indicating perfect impedance matching. In that case, antenna inductance and capacitance cancel each other. The antenna acts as a resistor whose resistance matches the antenna feed source. To match the impedance, the feed line and an accurate air gap between the patch and cavity ("g") play a vital role in impedance matching. The parametric analysis section shows the effect of "g" on antenna impedance matching. This combination allows an escalation in BW by merging two resonant frequencies by reducing the quality factor (Q-factor) down of the hybrid antenna. The ratio of the stored energy of the antenna's far-field region to the radiated power of the antenna is said to be Q-factor. The antenna being lossy, i.e., Q-factor down, means it can store less energy in its near-field region than the HMSIW antenna.

Conversely, it can radiate more energy. Consequently, this enhanced BW of the hybrid antenna surpasses the BW of the HMSIW antenna previously discussed in Section 2. The simulated BW and other associated parameters of the hybrid antenna will be discussed in Section 4 after comparing them with experimental data. A typical SIW does not support TM mode since it cannot provide continuous current along its side wall as it renders vias with a specific gap. As a result, the proposed HMSIW antenna excites TE_{101}, and later, outer patch gets excited by the same mode. Clearly, the TE_{101} radiation from each side of the patch gets ruled out by each other, as shown in Figure 4.

This phenomenon, thereupon, slightly reduces antenna gain and oppositely increases neat XPL in the boresight direction. Besides, the simulated surface current distribution with colourmap intensity is shown in Figure 5(b). The surface current is distributed throughout the antenna, therefore means the whole antenna is resonating. More importantly, the surface current intensity is low in the middle of the patch as the electric field magnitude is minimum shown already in Figure 4. Hence, it proves the existence of TE_{101} in the outer patch.

Furthermore, current intensity and direction at the patch also give an inkling about the mode and polarity of the electric field developed across the patch. This combination lets the antenna achieve a broader BW than the HMSIW antenna.

2.3. Parametric Analysis. To evaluate the frequency stability and the parameter's effect on the proposed antenna, several simulations were performed and shown in Figures 6(a) and 6(b). By fine-tuning each parameter, frequency shifting, BW, and the best response of S_{11} from this structure can be achieved, which is vivid by the parametric analysis shown

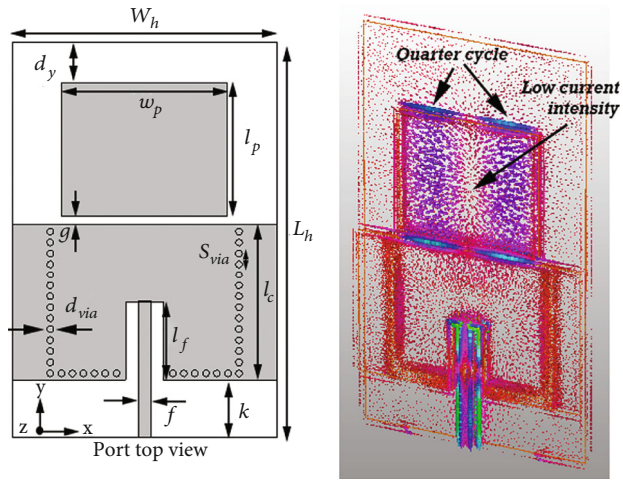

(a) (b)

FIGURE 5: The front layout of the hybrid antenna: (a) top view, where $L_h = 30$ mm, $W_h = 18$ mm, $d_y = 5.75$ mm, Wp = 11.13 mm, $l_f = 5.30$ mm, $d_{via} = 0.45$ mm, $S_{via} = 0.75$ mm, lp = 9.05 mm, $g = 0.53$ mm, lc = 10.70 mm, $r = 5.00$ mm, $f = 0.80$ mm, and $k = 3.9$ mm, and (b) current distribution.

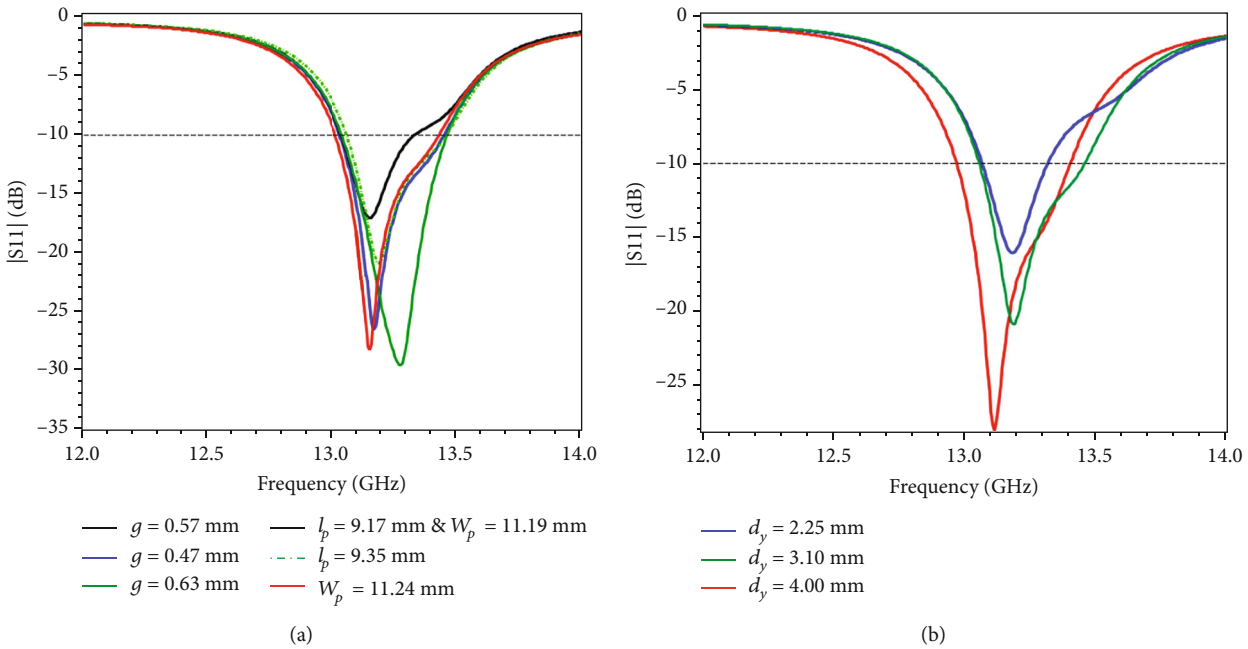

(a) (b)

FIGURE 6: The effect patch width "W_p," patch length "l_p," dielectric length "d_y," and distance "g" between the patch and cavity hybrid antenna reflection coefficient curve.

in Figure 6. The antenna's frequency stability is subject to antenna parameters; however, it appears almost stable irrespective of the slight parameter difference.

3. Design and Considerations

To construct a SIW cavity resonator, two conditions, $S_{via} \leq 2_{dvia}$ and $d_{via}/\lambda_0 \leq 0.1$, should be maintained where λ_0 is a free space wavelength. In this way, the SIW cavity acts like a metallic cavity shown [32, 36, 42, 43] and is able to prevent radiation leakage.

The above two rules go for a hybrid antenna in Figure 5(a), as its working frequency is the same as FMSIW. The radiation from HMSIW and hybrid antenna depends upon the mode generated inside the antenna. The working frequency of TE_{mnp} represented SIW resonator can be calculated by the following [34]:

$$f_{mnp} = \frac{1}{2\pi\sqrt{\mu\varepsilon}}\sqrt{\left(\frac{m\pi}{L_{eff}}\right)^2 + \left(\frac{n\pi}{h}\right)^2 + \left(\frac{n\pi}{W_{eff}}\right)^2}, \quad (1)$$

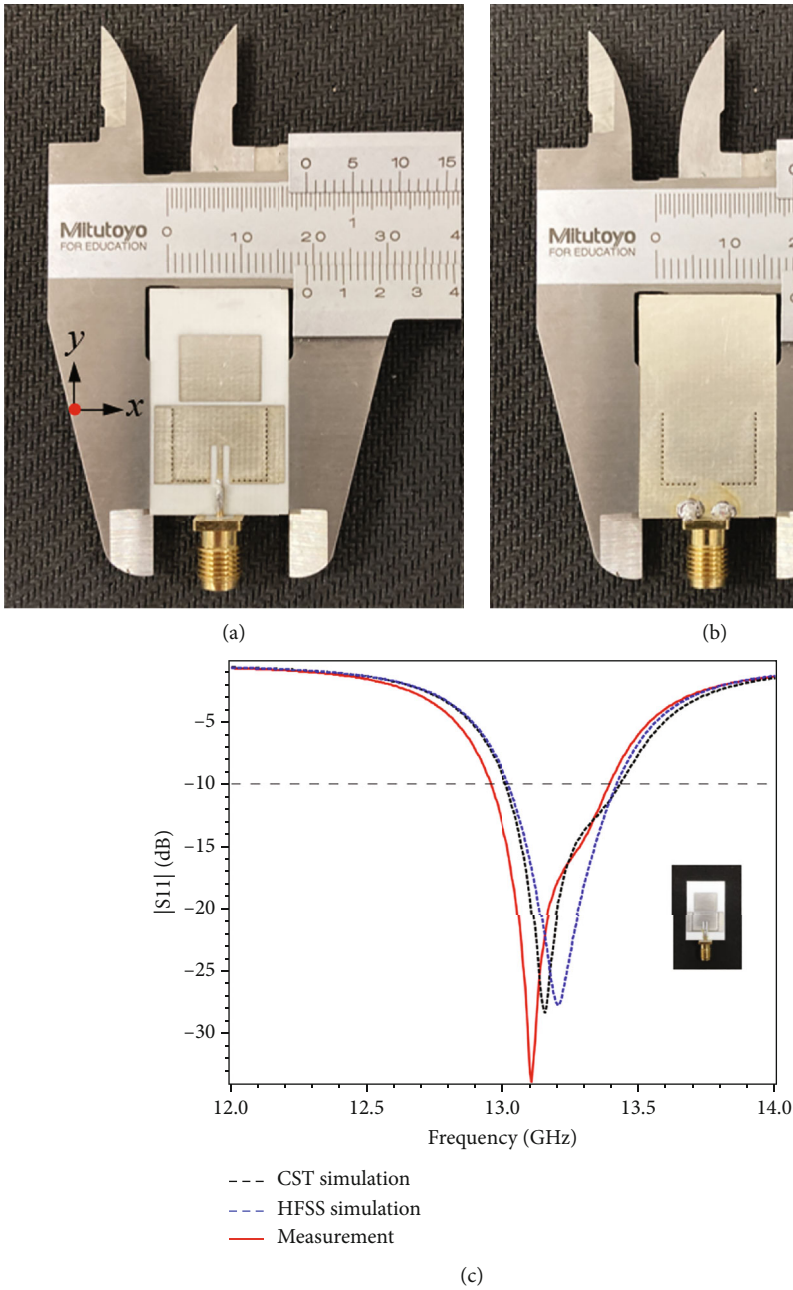

FIGURE 7: The fabricated sample of a hybrid antenna with slide caliper (mm) view: (a) front view and (b) rear view. (c) The measured S_{11} of a hybrid antenna compared with both CST and HFSS.

where $m = 1, 2$, $n = 1, 2, \cdots$, $p = 1, 2, \cdots$, $\mu = \mu_r\mu_o$, and $\varepsilon = \varepsilon_r\varepsilon_o$ indicate the permeability and permittivity of the chosen substrate of the SIW resonator, respectively. The equivalent length and width (L_{eff}, W_{eff}) can be determined by the following according to [9]

$$L_{\text{eff}} = l_{\text{siw}} - 1.08\frac{D^2}{S} + 0.1\frac{D^2}{l_{\text{siw}}}, \tag{2}$$

$$W_{\text{eff}} = w_{\text{siw}} - 1.08\frac{D^2}{S} + 0.1\frac{D^2}{w_{\text{siw}}}. \tag{3}$$

In (2) and (3), "D" represents the diameter of via and "s" represents the spacing between two adjacent via in SIW. In addition, the SIW possesses a large ratio of width to height that leads to $n = 0$ and resonates only TE_{m0p} modes. Figures 2 and 5(a) represent the radiated field for HMSIW and patch antenna, respectively. Additionally, the BW of the proposed antenna depends upon substrate thickness and the patch's dimension. The patch dimension was calculated utilizing the universal basic equation for patch antenna. To reduce surface wave and not make the antenna bulky, 0.8 mm was preferred as thickness. The initial assumption of the geometrical representation of FMSIW

Table 2: A comparison of both simulated and experimental data.

Parameters	Hybrid antenna	
	Simulated (13.12 GHz)	Measured (13.1 GHz)
S_{11}	-27.0 dB	-35.0 dB
BW	410 MHz	450 MHz
VSWR	1.02	N/A
Gain (dBi)	-3.09 (*E*), 6.06 (*H*)	6.45 (*E*), 6.24 (*H*)
SLL (dB)	-5.9 (*E*) -2.1 (*H*)	-7.93 (*E*), -2.56 (*H*)
XPL (dB)	-2.06 (*E*), -5.11 (*H*)	-1.56 (*E*), -4.07 (*H*)
Beam directions	359° (*E*), 44° (*H*)	358° (*E*), 309° (*H*)
HPBW	143.3° (*E*), 47.28° (*H*)	70.83° (*E*), 46.07° (*H*)
FTBR	12.59 dB	23.2 dB
E-field	15.2 dBV/m	N/A
H-field	-36.4 dBA/m	N/A
Radiated power	0.4163 W	N/A
Copper loss	0.01797 W	N/A
Dielectric loss	0.05220 W	N/A
Q-factor	32	29.11
Q_R	33.79	31.8
Rad. efficiency	94.68%	91.30
Total efficiency	92.36%	N/A

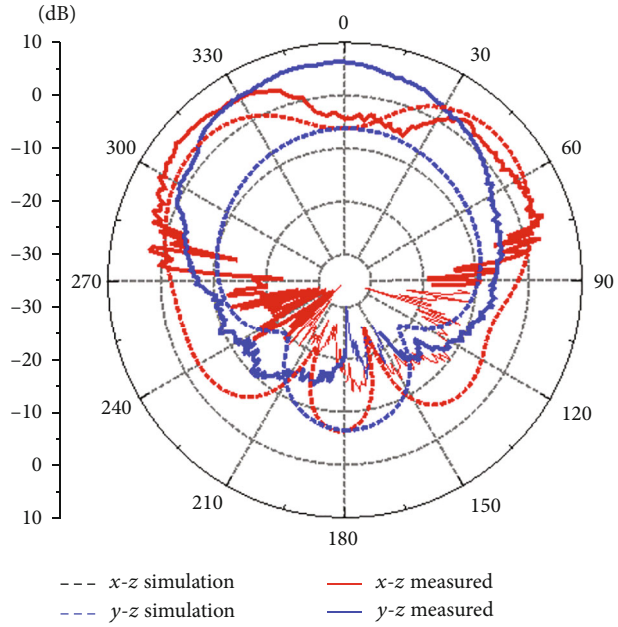

Figure 8: The normalized measured radiation patterns of a fabricated hybrid antenna in terms of *E*-plane (*YZ* cut) and *H*-plane (*XZ* cut).

was chosen arbitrarily, and its necessary mathematical calculation can be done using the equation discussed in [42].

4. Fabrication and Measurement Analysis

As per the simulation model built in the CST studio suite, this prototype was fabricated and tested using Rogers-RO4003C substrate ($\varepsilon_r = 3.2$) with a thickness of 32 mil. Figures 7(a) and 7(b) show photographs of a fabricated hybrid antenna. The experimental data maintains a good agreement with simulated data in Figure 7(c). Firstly, the fabricated sample has almost the same operating frequency of 13.1 GHz, similar to CST but in small disagreement with HFSS. Small discrepancy attributed to the fringing effect not counted in numerical simulation and an inaccurate air gap between the patches and HMSIW of a fabricated sample. Secondly, the measured S_{11} covers 12.93 GHz to 13.38 GHz after obtaining a BW of 450 MHz (3.46%), almost as similar to the simulation. This measured BW, however, is wider than the simulated BW of 410 MHz, which is vivid in Figure 7(c). This is because the *Q*-factor of the fabricated sample has decreased, which is 29.11, as reported in Table 2, due to the ohmic loss the antenna meets while soldering.

In addition to that, SMA connector loss and copper loss, which is often replaced by PEC in a simulation, are avoided. *Q*-factor can be determined by equation (4) and is directly related to antenna radiation efficiency, which is calculated using this equation (Table 2).

The measured normalized 2D polar plot radiation pattern at two planes is shown in Figure 8. The measured *E*-plane (*YZ* cut) pattern is as symmetrical as the simulated *E*-plane. The measured *E*-plane (E_θ in $\varphi = 90°$) points at 358° boresight direction, whereas the simulated *E*-plane is at 359° (Table 2).

$$Q_u = \frac{f_r}{\Delta f_{7dB}} = \eta_R Q_R. \tag{4}$$

Another overwhelming factor, HPBW, especially on *E*-plane, gets narrowed almost in halves compared to the simulated one reported in Table 2. This phenomenon also magnifies the incrementation in gain at *E*-plane (E_θ in $\varphi = 90°$) irrespective of some losses that could hamper antenna net gain. Alternatively, the *H*-plane (*XZ* cut) radiation pattern is as asymmetrical as the antenna structure, having almost equal two major lobes, with the main beam pointing at 309° boresight direction. The *H*-plane (E_θ in $\varphi = 0°$) gain is 6.24 dBi, whereas the simulated gain was 6.06 dBi (Table 2). Some losses can be attributed to coaxial cable loss during measurement. Needless to say, the absence of perfect alignment between the antenna under test and the standard horn antenna could affect the antenna gain and pattern. The measured SLL on *E*-plane (E_θ in $\varphi = 90°$) was found to be less than -7.90 dB (Table 2). However, SLL in *H*-plane is sole -2.1 dB in simulation and gets better by 0.5 dB in measurement due to the following reason. As previously mentioned, two major lobes are seen in the measured *H*-plane. One of them surpassed the simulated gain, ranging from 300 to 340° boresight direction. On the other hand, the other lobe, ranging from 30 to 60° boresight direction, becomes less dominant compared to the simulated one.

Since antennas gain increased in one direction while decreased in another, these two factors are responsible for achieving a better SLL in the *H*-plane than its corresponding

simulated value. The measured XPL values at E-plane (E_θ in $\varphi = 90^\circ$) and H-planes are -1.56 and -4.07, respectively. Although Section 2 predicted about dominating behaviour of XPL of this antenna, some loss while testing this antenna wreaks antenna XPL, and some discrepancy is seen in the corresponding simulation reported in Table 2. By employing a thin substrate, XPL could be suppressed. This elevated XPL in the fabricated sample also abates the radiation efficiency of the fabricated sample compared to the simulated, which is 91.30% (Table 2). The measured FTBR of the fabricated sample is mentioned in Table 2, where measured FTBR shows much better results than the simulated one. FTBR was found to be 23.3 dB at the resonant frequency, whereas simulated FTBR was only 12.59 dB. What is the main reason behind this?

Note that the antenna back lobe for both E-plane (E_θ in $\varphi = 90^\circ$) and H-plane (E_θ in $\varphi = 0^\circ$) in the measured radiation pattern completely disappears, which consequently pushes FTBR to its climax. The measured FTBR is spotted at more than 22 dB on its operating frequency range, which is meaningful, being a SIW antenna. Undoubtedly, Table 1 implies that the proposed antenna has improved FTBR, gain, and BW over recently published HMSIW, QMSIW, and SIW-based antenna. It conveys that SIW with a single patch provides promising results; further improvement, however, can be incorporated by dividing the patch into an array reported recently [42].

5. Conclusions

A novel cavity-backed hybrid antenna is proposed and tested experimentally. First, the HMSIW technique converts the nonradiating waveguide into a radiating antenna. Then, a patch of simple configuration is concatenated on the outer layer for the purpose of BW escalation. Both the parasitic patch and cavity-backed antenna are excited by TE_{101} mode of the antenna, where inset feed is used to excite antenna. Several antenna parameters, S_{11}, gain, BW, and XPL, have been investigated, and it shows elevated performances over recently published SIW-based antenna. Both simulated and measured data have a good agreement and proposed antenna.

Data Availability

Data can be given on demand.

Conflicts of Interest

The authors declare that they have no conflicts of interest.

Acknowledgments

The study is funded by the DRE (Director of Research and Extension) project of Chittagong University of Engineering and Technology (CUET), Bangladesh.

References

[1] I. Rosaline, A. Kumar, P. Upadhyay, and A. H. Murshed, "Four element MIMO antenna systems with decoupling lines for high-speed 5G wireless data communication," *International Journal of Antennas and Propagation*, vol. 2022, Article ID 9078929, 13 pages, 2022.

[2] T. Aboufoul, A. Alomainy, and C. Parini, "Polarisation reconfigurable ultra-wideband antenna for cognitive radio devices," in *Paper presented at: 2013 IEEE Antennas and Propagation Society International Symposium (APSURSI)*, pp. 1636-1637, Orlando, FL, USA, 2023.

[3] A. H. Murshed, M. A. Hossain, E. Nishiyama, and I. Toyoda, "Design and characterization of frequency reconfigurable honey bee antenna for cognitive radio application," *International Journal of Electrical and Computer Engineering*, vol. 12, no. 6, pp. 6178–6186, 2022.

[4] K. H. Sayidmarie and T. A. Nagem, "Compact dual-band dual-ring printed monopole antennas for WLAN applications," *Progress In Electromagnetics Research B*, vol. 43, pp. 313–331, 2012.

[5] A. H. Murshed, M. A. Hossain, M. A. Rahman, E. Nishiyama, and I. Toyoda, "Design and characterization of polarization reconfigurable heart shape monopole antenna for 2.4 GHz application," *International Journal of Electrical and Computer Engineering*, vol. 12, no. 4, pp. 3808–3819, 2022.

[6] A. Panahi, X. L. Bao, K. Yang, O. O'Conchubhair, and M. J. Ammann, "A simple polarization reconfigurable printed monopole antenna," *IEEE Transactions on Antennas and Propagation*, vol. 63, no. 11, pp. 5129–5134, 2015.

[7] C. A. Balanis, *Antenna Theory: Analysis and Design*, Wiley, Hoboken, NJ, USA, 2012.

[8] I. Garg, P. Bhartia, and I. J. Bahl, *Microstrip Antenna Design Handbook*, Artech House, Norwood, MA, USA, 2000.

[9] D. M. Pozar and S. M. Duffy, "A dual-band circularly polarized aperture-coupled stacked microstrip antenna for global positioning satellite," *IEEE Transactions on Antennas and Propagation*, vol. 45, no. 11, pp. 1618–1625, 1997.

[10] S. D. Targonski and D. M. Pozar, "Design of wideband circularly polarized aperture-coupled microstrip antennas," *IEEE Transactions on Antennas and Propagation*, vol. 41, no. 2, pp. 214–220, 1993.

[11] R. Przesmycki, M. Bugaj, L. Nowosielski, and M. Wnuk, "Wideband multilayer microstrip antenna: optimization of dielectric parameters on antenna bandwidth," in *Paper presented at: 2011 SBMO/IEEE MTT-S International Microwave and Optoelectronics Conference (IMOC 2011)*, pp. 217–220, Natal, Brazil, 2011.

[12] C. Y. Huang, J. Y. Wu, and K. L. Wong, "Cross-slot-coupled microstrip antenna and dielectric resonator antenna for circular polarization," *IEEE Transactions on Antennas and Propagation*, vol. 47, no. 4, pp. 605–609, 1999.

[13] A. H. Murshed, M. A. Hossain, M. A. Rahman, E. Nishiyama, and I. Toyoda, "Designing of a both-sided MIC starfish microstrip array antenna for K-band application," in *Paper presented at: 2021 IEEE Region 10 Symposium (TENSYMP)*, Jeju, Republic of Korea, 2021.

[14] P. Chowdhury, N. Chakma, A. H. Murshed, M. A. Hossain, and Q. D. Hossain, "An improved 2×2 array antenna using both-sided microwave integrated circuit technology for circular polarization," *International Journal of Electrical and Computer Engineering*, vol. 13, no. 1, pp. 619–628, 2023.

[15] M. A. Hossain, A. H. Murshed, M. A. Rahman, E. Nishiyama, and I. Toyoda, "A gain enhanced linear polarization switchable array antenna with switching diodes," *International Journal of Electrical and Computer Engineering*, vol. 32, no. 10, pp. 1–9, 2022.

[16] S. Ershadi, A. Keshtkar, A. H. Abdelrahman, and H. Xin, "Wideband high gain antenna subarray for 5G applications," *Progress In Electromagnetics Research C*, vol. 78, pp. 33–46, 2017.

[17] G. J. Hirokawa, H. Arai, and N. Goto, "Cavity-backed wide slot antenna," *Proceedings of the Institution of Electrical Engineers*, vol. 136, no. 1, pp. 29–33, 1989.

[18] G. J. H. Nakano, M. Iwatsuki, M. Sakurai, and J. Yamauchi, "A cavity-backed rectangular aperture antenna with application to a tilted fan beam array antenna," *IEEE Transactions on Antennas and Propagation*, vol. 51, no. 4, pp. 712–718, 2003.

[19] A. T. Adams, "Flush mounted rectangular cavity slot antennas theory and design," *IEEE Transactions on Antennas and Propagation*, vol. 15, no. 3, pp. 342–351, 1967.

[20] W. Hong, N. Behdad, and K. Sarabandi, "Size reduction of cavity backed slot antennas," *IEEE Transactions on Antennas and Propagation*, vol. 54, no. 5, pp. 1461–1466, 2006.

[21] Z. Chen and Z. Shen, "A compact cavity-backed end-fire slot antenna," *IEEE Antennas and Wireless Propagation Letters*, vol. 13, pp. 281–284, 2014.

[22] X. Li, J. Xiao, Z. Qi, and H. Zhu, "Broadband and high-gain SIW-fed antenna array for 5G applications," *IEEE Access*, vol. 6, pp. 56282–56289, 2018.

[23] J. Wu, Y. J. Cheng, and Y. Fan, "A wideband high-gain high-efficiency hybrid integrated plate array antenna for V-band inter-satellite links," *IEEE Transactions on Antennas and Propagation*, vol. 63, no. 4, pp. 1225–1233, 2015.

[24] A. Kumar and S. Dwari, "Substrate integrated waveguide cavity-backed self-triplexing slot antenna," *IEEE Antennas and Wireless Propagation Letters*, vol. 16, pp. 3249–3252, 2017.

[25] G. Q. Luo, Z. F. Hu, Y. Liang, L. Y. Yu, and L. L. Sun, "Development of low profile cavity backed crossed slot antennas for planar integration," *IEEE Transactions on Antennas and Propagation*, vol. 57, no. 10, pp. 2972–2979, 2009.

[26] S. Mukherjee, A. Biswas, and K. V. Srivastava, "Broadband substrate integrated waveguide cavity-backed bow-tie slot antenna," *IEEE Antennas and Wireless Propagation Letters*, vol. 13, pp. 1152–1155, 2014.

[27] T. Zhang, W. Hong, Y. Zhang, and K. Wu, "Design and analysis of SIW cavity backed dual-band antennas with a dual-mode triangular-ring slot," *IEEE Transactions on Antennas and Propagation*, vol. 62, no. 10, pp. 5007–5016, 2014.

[28] G. Q. Luo, Z. F. Hu, L. X. Dong, and L. L. Sun, "Planar slot antenna backed by substrate integrated waveguide cavity," *IEEE Antennas and Wireless Propagation Letters*, vol. 7, pp. 236–239, 2008.

[29] A. B. Terki, M. Nedil, and Y. B. Chaouche, "Design of compact UWB coplanar waveguide-fed modified Sierpinski carpet fractal antenna," in *2019 IEEE International Symposium on Antennas and Propagation and USNC-URSI Radio Science Meeting*, Atlanta, GA, USA, 2019.

[30] S. Tripathi, A. Mohan, and S. Yadav, "A compact Koch fractal UWB MIMO antenna with WLAN band-rejection," *IEEE Antennas and Wireless Propagation Letters*, vol. 14, pp. 1565–1568, 2015.

[31] O. Caytan, S. Lemey, S. Agneessens et al., "Half-mode substrate-integrated-waveguide cavity-backed slot antenna on cork substrate," *IEEE Antennas and Wireless Propagation Letters*, vol. 15, pp. 162–165, 2016.

[32] X. Yang, L. Ge, Y. Ji, X. Zeng, and K. M. Luk, "Design of low-profile multi-band half-mode substrate-integrated waveguide antennas," *IEEE Transactions on Antennas and Propagation*, vol. 67, no. 10, pp. 6639–6644, 2019.

[33] N. C. Pradhan, K. S. Subramanian, R. K. Barik, and Q. S. Cheng, "A shielded-QMSIW-based self-diplexing antenna for closely spaced bands and high isolation," *IEEE Antennas and Wireless Propagation Letters*, vol. 20, no. 12, pp. 2382–2386, 2021.

[34] A. Iqbal, M. Al-Hasan, I. B. Mabrouk, and M. Nedil, "Ultra-compact quarter-mode substrate integrated waveguide self-diplexing antenna," *IEEE Antennas and Wireless Propagation Letters*, vol. 20, no. 7, pp. 1269–1273, 2021.

[35] J. H. M. Mujumdar and A. Alphones, "Eighth-mode substrate integrated resonator antenna at 2.4 GHz," *IEEE Antennas and Wireless Propagation Letterst*, vol. 15, pp. 853–856, 2016.

[36] A. T. M. Bozzi, A. Georgiadis, and K. Wu, "Review of substrate integrated waveguide circuits and antennas," *IET Microwaves, Antennas & Propagation*, vol. 5, no. 8, pp. 909–920, 2011.

[37] S. Priya, K. Kumar, S. Dwari, and M. K. Mandal, "Circularly polarized self-diplexing SIW cavity backed slot antennas," *IEEE Transactions on Antennas and Propagation*, vol. 68, no. 3, pp. 2387–2392, 2020.

[38] S. Priya and S. Dwari, "A compact self-triplexing antenna using HMSIW cavity," *IEEE Antennas and Wireless Propagation Letters*, vol. 19, no. 5, pp. 861–865, 2020.

[39] M. Donelli, S. K. Menon, G. Marchi, V. Mulloni, and M. Manekiya, "Design of an ultra wide band antenna based on a SIW resonator," *Progress In Electromagnetics Research C*, vol. 103, pp. 187–197, 2020.

[40] J. Qi, Q. Wang, F. Deng, Z. Zeng, and J. Qiu, "Low-profile uni-cavity high-gain FPC antenna covering entire global 2.4 GHz and 5 GHz WiFi-bands using uncorrelated dual-band PRS and phase compensation AMC," *IEEE Transactions on Antennas and Propagation*, vol. 70, no. 11, pp. 10187–10198, 2022.

[41] J. Xu, Z. N. Chen, X. Qing, and W. Hong, "Bandwidth enhancement for a 60 GHz substrate integrated waveguide fed cavity array antenna on LTCC," *IEEE Transactions on Antennas and Propagation*, vol. 59, no. 3, pp. 826–832, 2011.

[42] A. H. Murshed, M. A. Hossain, N. K. Kiem et al., "A half-mode cavity backed hybrid array antenna using substrate integrated waveguide (SIW) technology," *IEEE Transactions on Antennas and Propagation*, vol. 71, no. 1, pp. 169–179, 2023.

[43] H. Dashti and M. H. Neshati, "Development of low-profile patch and semi-circular SIW cavity hybrid antennas," *IEEE Transactions on Antennas and Propagation*, vol. 62, no. 9, pp. 4481–4488, 2014.

[44] W. P. Hung, T. H. Lee, and C. H. Chang, "Non-invasive detection of object by UWB radar," in *2017 Asia-Pacific International Symposium on Electromagnetic Compatibility (APEMC)*, Seoul, Korea, 2017.

[45] F. Challita, P. Laly, M. Yusuf et al., "Massive MIMO communication strategy using polarization diversity for industrial scenarios," *IEEE Antennas and Wireless Propagation Letters*, vol. 19, no. 2, pp. 297–301, 2019.

[46] R. O. R. Jenssen, M. Eckerstorfer, and S. Jacobsen, "Drone-mounted ultrawideband radar for retrieval of snowpack

properties," *IEEE Transactions on Instrumentation and Measurement*, vol. 69, no. 1, pp. 221–230, 2020.

[47] S. Wu, T. Sakamoto, K. Oishi et al., "Person-specific heart rate estimation with ultra-wideband radar using convolutional neural networks," *IEEE Access*, vol. 7, pp. 168484–168494, 2019.

[48] N. K. Mallat and A. Iqbal, "Substrate integrated waveguide-based simultaneous transmit and receive antenna for full-duplex wearable devices," *International Journal of Antennas and Propagation*, vol. 32, no. 7, Article ID e23188, 2022.

[49] U. Naeem, A. Iqbal, M. F. Shafique, and S. Bila, "Efficient design methodology for a complex DRA-SIW filter-antenna subsystem," *International Journal of Antennas and Propagation*, vol. 2017, Article ID 6401810, 9 pages, 2017.